Article:
Mojtabaei, S.M. orcid.org/0000-0002-4876-4857, Yilmaz, F., Becque, J. et al. (1 more author) (2023) Lateral performance of cold-formed steel OSB-sheathed stud wall panels. ce/papers, 6 (3-4). pp. 1965-1971. ISSN 2509-7075

https://doi.org/10.1002/cepa.2706

ce/papers Proceedings in civil engineering

Ernst & Sohn A Wiley Brand

eurosteel AMSTERDAM 2023

Ernst & Sohn A Wiley Brand

Lateral performance of cold-formed steel OSB-sheathed stud wall panels

Seyed Mohammad Mojtabaei[1,2], Fatih Yilmaz[2], Jurgen Becque[3], Iman Hajirasouliha[2]

1 Introduction

Cold-formed steel (CFS) has become a popular construction material due to its consistent quality, ease of mass production, lightweight, and quick installation [1-3]. CFS is commonly used in the construction of low- to medium-rise buildings and moment-resisting portal frames [4-5]. CFS buildings typically require an additional lateral load-resisting system, which can be provided by strap-bracing or shear walls [6]. However, current design standards (e.g. the Eurocode [7]) do not allow designers to take advantage of the inherent capacity and stiffness provided by the boards used to clad CFS stud walls. More research is needed to develop appropriate design methodologies, particularly in seismic regions, where the increased demands on lateral load-resisting systems require higher capacity, ductility, and energy dissipation, and where the overall seismic performance of CFS structures can be negatively affected by instabilities and premature failure of thin-walled elements and connections [8].

Several numerical and experimental research studies have focused on the lateral behaviour and design of sheathed wall panels. Badr et al. [9] conducted experiments and numerical simulations to investigate the increase in lateral stiffness and strength resulting from adding X-bracing and fibre cement boards. Additionally, it was found that the presence of noggin members delayed buckling of the studs and reduced their twisting deformations. Pan and Shan [10] compared the lateral behaviour of unsheathed CFS wall panels to those sheathed with gypsum board, Calcium Silicate Board (CSB), and Oriented Strand Board (OSB). They observed that most walls experienced bearing failure and separation of the sheathing from the frame at the locations of the self-drilling screws. Among the sheathing materials, OSB provided the highest lateral strength, while gypsum boards provided the highest ductility. Ye et al. [11] experimentally investigated the seismic performance of CFS shear wall panels with double-layer gypsum board, Bolivian magnesium board, and CSB under cyclic lateral loading conditions. They recommended that gypsum board and CSB should only be used in low-seismicity regions.

In this study, detailed nonlinear finite element (FE) models of OSB-sheathed CFS wall panels were developed, of which the predicted load-displacement responses and failure modes were first validated against experimental data.

https://doi.org/10.1002/cepa.2706 wileyonlinelibrary.com/journal/cepa

The validated models were subsequently used to conduct comprehensive parametric studies to investigate the influence of key design variables, including the OSB thickness, the CFS thickness and the board configuration. Based on the lateral load-displacement responses obtained from the FE models, the structural performance parameters, such as lateral load capacity and initial stiffness, as well as the governing seismic characteristics were compared.

2 Modelling Assumptions and Validation

Detailed FE models were developed using the ABAQUS software [12] in order to predict the behaviour and failure modes of sheathed CFS shear wall panels with a high level of accuracy. The models were validated against experimental data reported by Blais and Rogers [13], pertaining to three CFS wall panels clad on one side with OSB (Fig. 1). The overall dimensions of the shear walls were 1220×2440 mm × mm. The CFS framing elements were composed of U-shaped tracks and lipped-C studs with dimensions of 92.1 × 31.8 × 1.09 (mm) and 92.1 × 41.3 × 12.7 × 1.09 (mm), respectively. The study used self-drilling screws to connect the OSB sheathing to the framing and Simpson Strong-Tie S/HD10 hold-down devices to control overturning moments on the shear wall. The CFS top track was subjected to an in-plane lateral displacement during the test to generate the loading. The FE models took into account material and geometric nonlinearity, initial geometric imperfections, contact interaction between the constituent elements of the panel, and realistic nonlinear behaviour of the fasteners.

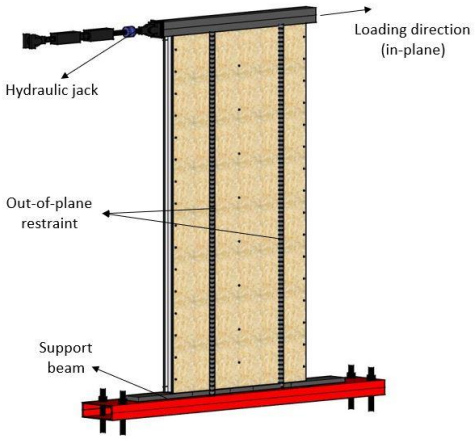

Figure 1 Experimental set-up used by Blais [13]

2.1 Modelling of screws

The behaviour of the screws between the CFS framing members and the OSB has a significant influence on the lateral performance and failure mode of the sheathed panels, as shown in previous experimental studies [13]. The empirical equations proposed by Kyvelou et al. [14] were implemented in the FE models to establish the in-plane load-slip response of the screws:

$$s = \frac{P}{K_0} + C_1\left(\frac{P}{P_5}\right)^{C_2} \quad (1)$$

$$C_1 = s_5 - \frac{P_5}{K_0} \quad (2)$$

$$C_2 = \frac{ln\left(S_b - \frac{P_b}{K_0}\right) - ln\,(C_1)}{ln\left(\frac{P_b}{P_5}\right)} \quad (3)$$

In the above equations, K_0 is the slip modulus of the screws and C_1 and C_2 are coefficients. The value of S_5 was taken as 5 mm, as suggested by Kyprianou et al. [15], and P_5 is the slip load corresponding to S_5. P_b is the bearing resistance of the board in contact with the fastener, which is calculated by multiplying the compressive strength of the board with the area of the board in contact with the fastener, and S_b is the slip corresponding to P_b. These parameters were obtained from push-out tests conducted by Peterman and Schafer [16], and a summary is provided in Table 1. The in-plane load-slip response of the screws was calculated using the aforementioned Eqs. (1-3) is also compared to the test results in Fig. 2. It can be seen that the predicted response agrees well with the experimental data up to the peak capacity.

Table 1 Parameters describing in-plane load-slip response of the fasteners [16]

Material	K_0 (kN/mm)	P_b (kN)	S_b (mm)	P_5 (kN)	S_5 (mm)	P_v (kN)
OSB	1.90	0.67	0.37	1.90	5	2.03

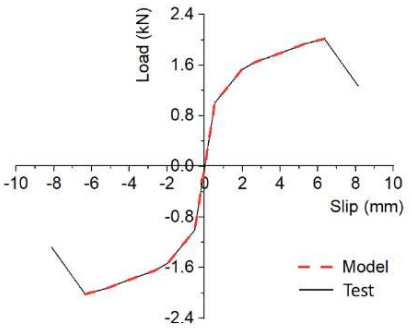

Figure 2 Comparison between load-slip response of the fasteners obtained from push-out tests [16] and the numerical prediction [14]

Previous studies have shown that the screw spacing and the CFS thickness have a negligible effect on the connection behaviour [16] since damage initiates in the board material rather than in the CFS. Conversely, however, the board thickness plays an important role, and it was found that the slip modulus and strength of the connections increase linearly with increasing board thickness [17]. These findings were used to adjust the load-slip relationship of the screws depending on the OSB thickness, resulting in the graphs in Fig. 3. It is noted that the experimentally measured post-peak response of the connections was added to the pre-peak behaviour obtained from the empirical equations proposed by Kyvelou et al. [14] in order to obtain a model over the full deformation range for input into the FE models.

The self-drilling screws were modelled using discrete fastener elements, available in the Abaqus library [12]. The fastener elements were assigned a radius of influence, equal to the radius of the screw. Mesh-independent fastening points were connected using attachment lines that allowed for the input of the inelastic bearing and pull-out behaviour.

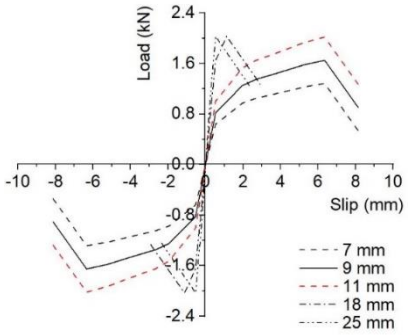

Figure 3 Behaviour of screws connecting CFS to OSB with different thicknesses

2.2 Element type and mesh density

The CFS members and sheathing were modelled using S4R shell elements. This type of element has been proven to be reliable in predicting the flexural and membrane behaviour of thin-walled structures over a wide range of applications [18]. However, the mesh density can have a significant impact on the accuracy of the results. To obtain an appropriate balance between accuracy and computational cost, a mesh study was conducted, after which a mesh size of 15×15 mm^2 was assigned to the components of the model.

2.3 Material modelling

The material properties of the CFS and the OSB used in the FE models were obtained from coupon tests [13] and are presented in Tables 2 and 3. The Young's moduli of the CFS and the OSB are denoted by E_{CFS} and E_{OSB} respectively, while σ_y and σ_u are the yield stress and the tensile strength of the CFS. $\sigma_{t,OSB}$ and $\sigma_{c,OSB}$ denote the ultimate tensile and compressive stresses of the OSB, and ε_u and $\varepsilon_{c,OSB}$ are the corresponding strain values. The Poisson ratios of the CFS and the OSB are represented by υ_{CFS} and υ_{OSB}, respectively. To account for the effects of large inelastic strains, the engineering stress-strain curve of the CFS was converted into the true stress versus true plastic strain curve. It is noted that the effects of cold-working (i.e. strain hardening and residual stress) in the rounded corner zones of the CFS studs and tracks were neglected in this study. These effects are usually quite moderate in CFS and, to some extent, negate each other [19].

Table 2 Measured material properties of the CFS

Specimens	E_{CFS} (GPa)	υ_{CFS}	σ_y (MPa)	σ_u (MPa)	ε_u
CFS	199	0.3	264	345	0.315

Table 3 Measured material properties of the OSB

Specimens	E_{OSB} (MPa)	υ_{OSB}	$\sigma_{t,OSB}$ (MPa)	$\sigma_{c,OSB}$ (MPa)	$\varepsilon_{c,OSB}$
OSB	3650	0.2	11.9	14.1	0.006

2.4 Geometric imperfections

Global buckling of the CFS elements was prevented by the presence of the boards [13], which shifted the governing failure mode in the CFS to cross-sectional instability. To incorporate imperfections into the model, an elastic buckling analysis was carried out on the sheathed wall panel, and the scaled first eigenmode was used as the shape of the initial geometric imperfections. The amplitude of the imperfections was determined based on the work by Schafer and Peköz [20], and the values adopted were $0.34t$ and $0.94t$ for the local and distortional imperfections, respectively.

2.5 Boundary and loading conditions

Fig. 4 shows the boundary conditions and loading applied to the FE models. The flange-to-web corners of the top track were restrained in the out-of-plane direction and laterally loaded in a displacement-controlled manner. The bottom track was connected to a rigid plate using 'tie' constraints at the locations of the anchor bolts. The hold-downs were tied to the chord and track elements. Between CFS elements a surface-to-surface 'hard' contact was defined in the normal direction and a friction coefficient of 0.2 was specified in the tangential direction. This approach closely resembles the methodology employed by Hasanali et al. [21]. A sensitivity analysis showed that varying this coefficient between 0.1 and 0.25 had a minor influence on the load-displacement response of the panel, resulting in a variation of about 2.5% in the peak load.

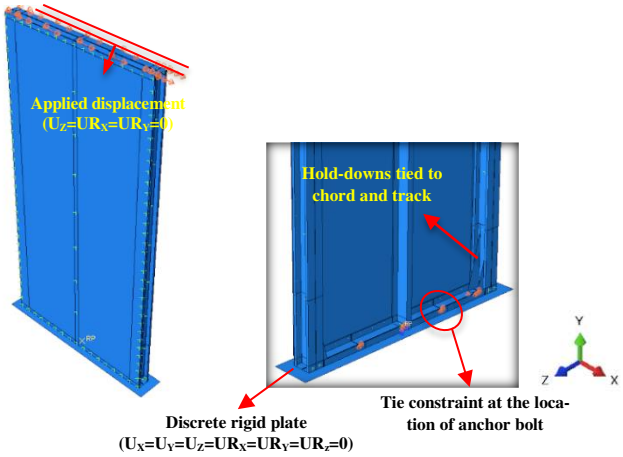

Figure 4 Boundary and loading conditions

2.6 Model Validation

Nonlinear 'Static General' analyses were carried out and the results of these analyses were compared to the experimental data obtained by Blais [13]. Fig. 5 shows the lateral load versus the horizontal displacement of the top track, obtained from the FE models and the experiments, for screw spacings of 75, 100, and 152 mm. In addition, the ratios of various FE-predicted parameter values to their experimental counterparts are listed in Table 4, accompanied by their respective statistical indicators. These parameters include the lateral load capacity ($F_{Max,FE}/F_{Max,Exp}$), the initial tangent stiffness ($S_{i,FE}/S_{i,Exp}$), and the ultimate lateral displacement ($\Delta_{u,FE}/\Delta_{u,Exp}$). The ultimate displacement of the panel was defined as the displacement at which the load had dropped by 20% from its peak value, following the recommendation of AISC 341-16 [22]. The FE model results showed a good agreement with the experimental data across all parameters, with a typical error of 3%. The failure modes predicted by the FE models were consistent with those observed in the experiments. Fig. 6

shows the Von Mises stresses in the boards at failure. The grey zones indicate material failure (i.e. crushing) in the boards, deduced based on the stress-strain curve of the OSB material and a Von Mises criterion. These areas are primarily located around the fasteners, resulting from bearing action, and in some instances extend all the way from the connection to the board's edge, indicating possible block/plug tear-out. This is entirely consistent with the experimental investigation, which reported a combination of connector pull-through and block/plug tear-out at the corners as the observed failure mechanism. It should be noted that local buckling of the bottom track near the hold-downs was also observed in the FE model, although no mention of this was found in the experimental report.

Table 4 Comparison between experimental results [13] and FE predictions for wall panels with different screw spacing

Screw spacing	$F_{Max,FE}/F_{Max,Exp}$	$\Delta_{u,FE}/\Delta_{u,Exp}$	$S_{i,FE}/S_{i,Exp}$
75 mm	0.99	1.00	0.99
100 mm	0.93	0.97	0.92
152 mm	1.01	0.95	0.94
Average error	3%	3%	5%
St. deviation	0.042	0.025	0.036

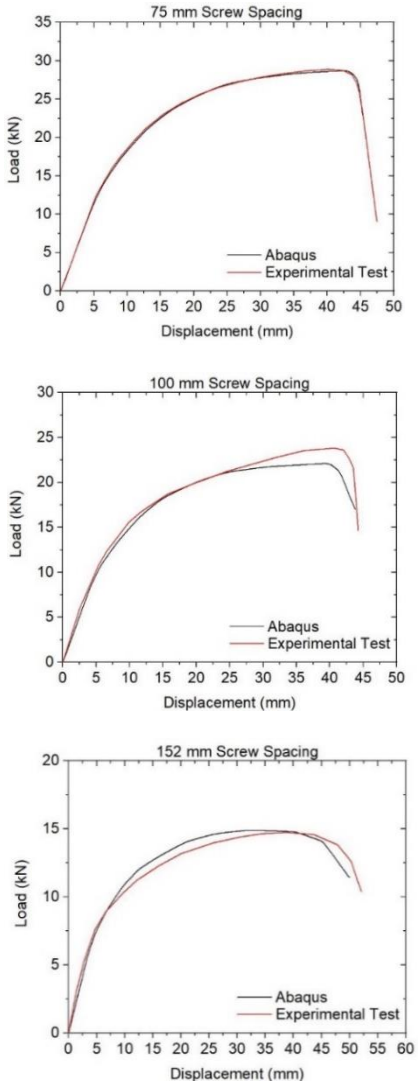

Figure 5 Load-displacement curves of wall panels with different screw spacing, obtained from FE models and experiments [13]

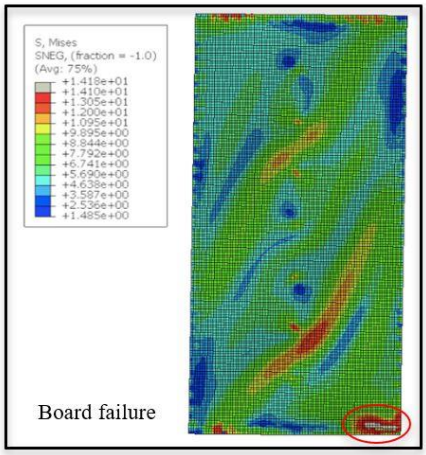

Figure 6 Von Mises stress distribution in the boards at failure

3 Parametric study

The validated FE models were further utilized to carry out a parametric study of the structural behaviour of OSB-sheathed CFS stud wall panels with different OSB and CFS thicknesses, and board configurations. This part of the study focused on two specific performance parameters, namely the lateral load capacity and the initial stiffness.

3.1 Design variables

Table 5 presents the details of the parametric studies, including the selected design variables. Three CFS element thicknesses (1.09, 1.5, 2, and 3 mm) were considered, as well as five OSB thicknesses (7, 9, 11, 18, and 25 mm), and four board configurations (A to D), which are further detailed in Fig. 7. The experimentally tested stud wall with board configuration A and OSB and CFS thicknesses of 9 mm and 1.09 mm, respectively, were used as the "benchmark specimen" for comparative purposes.

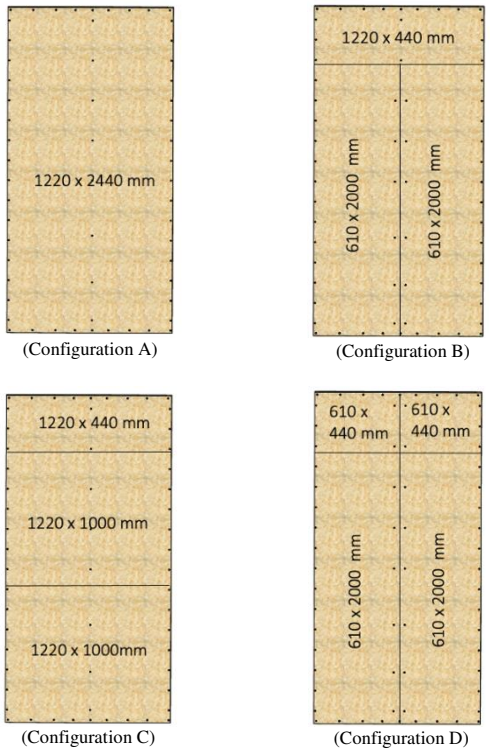

Figure 7 Board configurations used in parametric studies

Table 5 Design variables in parametric studies

Variables	Value
OSB thickness	7, 9, 11, 18, 25 mm
CFS thickness	1.09, 1.5, 2.0, 3.0 mm
Board configuration	A, B, C, D

3.2 Results

The load-displacement responses of the CFS stud wall panels included in the parametric study are compared to the benchmark specimen in Fig. 8. The capacity of the wall was determined from either the peak of the load vs. lateral displacement curve, or crushing of the board material, whichever occurred first.

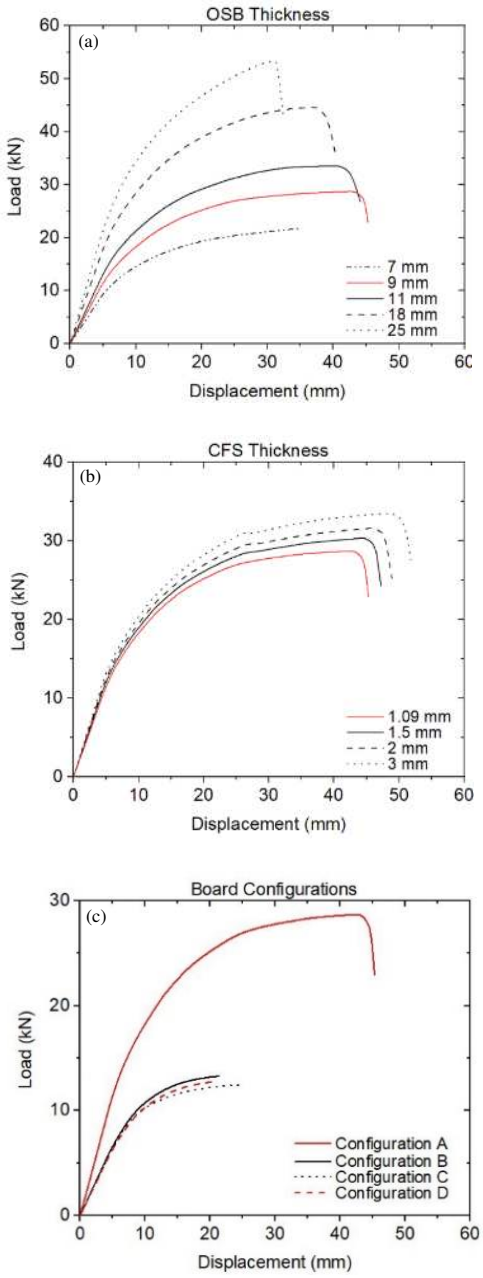

Figure 8 Load-displacement responses of stud wall panels with various design variables

3.2.1 *OSB and CFS thicknesses*

Fig. 8(a) demonstrates that the thickness of the OSB significantly affects the overall load-displacement response of the wall panels. The numerical findings are summarized in Fig. 9, indicating a 55% improvement in both the maximum capacity (F_{max}) and initial stiffness (S_i) over the benchmark specimen when doubling the OSB thickness from 9 to 18 mm. In contrast, the CFS thickness has a relatively minor effect on the lateral behaviour of the panels (Fig. 8(b)). Increasing the CFS frame thickness from 1.09 mm to 2 mm only provided a 10% enhancement in lateral capacity and initial stiffness, as also shown in Fig. 10.

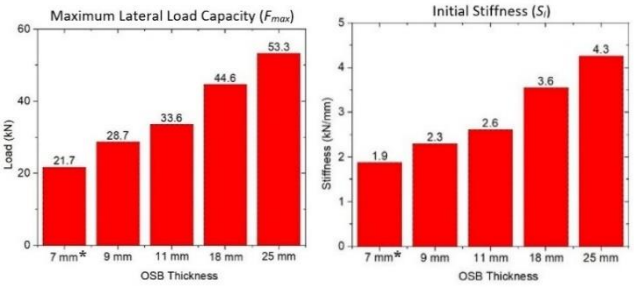

Figure 9 Performance parameters of OSB-sheathed CFS wall panels with different OSB thicknesses (*benchmark specimen)

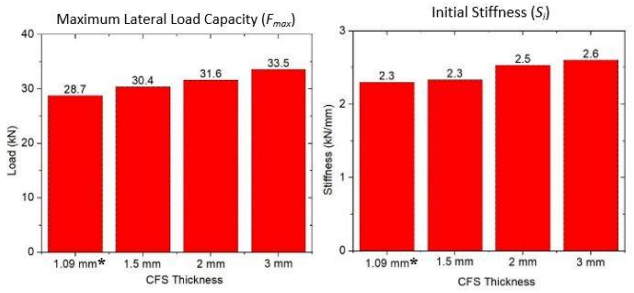

Figure 10 Performance parameters of OSB-sheathed CFS wall panels with different CFS thicknesses (*benchmark specimen)

3.2.2 *Board configuration*

The findings presented in Fig. 8(c) demonstrate a notable influence of the layout configuration of the OSB boards on the lateral load-displacement response. This relationship is further illustrated in Fig. 11, which highlights that the inclusion of horizontal or vertical seams in the boards resulted in a significant decrease in both lateral strength and stiffness, with reductions of up to 60% observed for the analysed configurations. In wall panels with a horizontal seam, the complete hori-zontal shear force in the seam has to be resisted by the CFS studs alone, leading to localized yielding and shear failure of the studs. Both configurations B and C also experienced local buckling of the boards, causing the seams to separate, and localized crushing of the OSB in the corners of the subpanels. Subdividing the boards to introduce additional seams in Configuration D had a neg-ligible additional impact on the overall lateral behaviour of the wall panel and resulted in identical failure mecha-nisms.

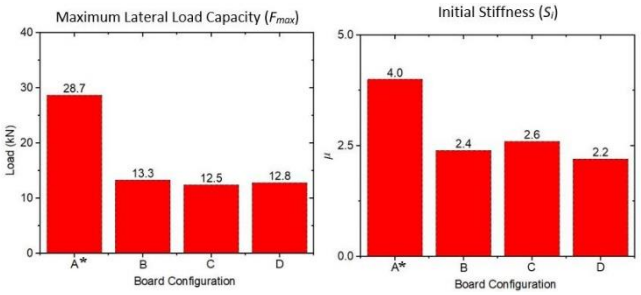

Figure 11 Performance parameters of OSB-sheathed CFS wall panels with different board configurations (*benchmark specimen)

4 Seismic performance characteristics

Additional parametric studies were carried out to assess the seismic performance characteristics of OSB-sheathed CFS wall panels and investigate the impact of key design variables on the following seismic performance parameters:

(i) deformation capacity, as measured by the ultimate displacement (Δ_u), defined as the displacement at which the residual post-peak capacity reduces to 80%, or the displacement when crushing of the boards occurs (whichever happens first).

(ii) ductility, which indicates the ability of a structure to undergo substantial plastic deformations without a significant reduction in its load-carrying capacity [23]. The most widely accepted measure of ductility (μ) is the ratio of the ultimate displacement (Δ_u) to the yield displacement (Δ_y):

$$\mu = \frac{\Delta_u}{\Delta_y} > 1.0 \quad (4)$$

To determine the yield displacement (Δ_y) in Eq. (4), the load-displacement curve was transformed into an equivalent bi-linear curve via the widely recognized Equivalent Energy Elastic-Plastic (EEEP) idealization method, which is endorsed by the AISC 341 [22].

(iii) energy dissipation capacity (E), quantified as the area under the equivalent bi-linear load-displacement curve up to the ultimate displacement (Δ_u).

Table 6 shows the ultimate displacements (Δ_u), ductility ratios (μ) and energy dissipation capacities (E) obtained from the numerical models for wall panels with various design variables. Table 6 indicates that using thinner OSB led to higher ductility and ultimate displacements. A difference of 40% in both variables was observed between configurations with thicknesses of 9 and 25 mm. Furthermore, thicker OSB generally leads to higher energy dissipation capacities. It is also seen in Table 6 that using thicker CFS elements consistently improved the seismic characteristics of the OSB-sheathed wall panels in terms of ultimate displacement, ductility and energy dissipation capacity. This is due to the delay of instabilities.

The seismic characteristics of the wall panels are significantly affected by the board layout configuration, as demonstrated by Table 6. The presence of seams in the sheathing (i.e. configurations B, C and D) resulted in unfavourable seismic characteristics, due to the occurrence of localised failure in the vertical CFS elements at the location of those seams. The results demonstrated that the lateral strength, ductility and energy dissipation were reduced by up to 60%, 45% and 55% respectively compared to the system with no seam (configuration A).

Table 6 Comparison between seismic characteristics of wall panels with various design variables (*benchmark specimen)

Design Variables		Δ_u (mm)	μ	E (J)
OSB thickness	7 mm	35	3.5	568
	*9 mm	45	4.0	1026
	11 mm	44	3.8	1154
	18 mm	40	3.6	1374
	25 mm	32	2.9	1271
CFS thickness	*1.09 mm	45	4.0	1026
	1.5 mm	48	4.1	1129
	2 mm	49	4.4	1221
	3 mm	52	4.5	1383
Board configuration	*A	45	4.0	1026
	B	21	2.4	204
	C	25	2.6	231
	D	21	2.2	201

5 Conclusions

Using validated FE models, a comprehensive parametric study was carried out to investigate the structural performance parameters of OSB-clad CFS stud walls under lateral in-plane loading. The study showed the thickness of the OSB sheathing to be a design parameter of primordial importance. Thicker OSB improved the lateral capacity and initial stiffness of the panels almost proportionally. With respect to seismic performance, thinner OSB provided higher ductility and ultimate displacements, but thicker OSB significantly increased the energy dissipation. The effect of the thickness of the CFS frame members on the lateral strength and stiffness was rather small, but thicker CFS elements improved the seismic characteristics due to increased plasticity. The presence of horizontal or vertical seams in the boards significantly reduced the lateral capacity and stiffness of the system, due to localised failure occurring at the seams. It also had a very detrimental effect on the energy dissipation capacity of the system.

References

[1] Mojtabaei, S.M.; Becque, J.; Hajirasouliha, I. (2021) *Structural Size Optimization of Single and Built-Up Cold-Formed Steel Beam-Column Members*. Journal of Structural Engineering, 147(4), p.04021030.

[2] Hasanali, M.; Roy, K.; Mojtabaei, S.M.; Hajirasouliha, I.; Clifton, G.C.; Lim, J.B.P. (2022) *A critical review of cold-formed steel seismic resistant systems: Recent developments, challenges and future directions*. Thin-Walled Structures 180, 109953.

[3] Schafer, B.W.; Ayhan, D.; Leng, J.; Liu, P.; Padilla-Llano, D.; Peterman, K.D.; Stehman, M.; Buonopane, S.G.; Eatherton, M.; Madsen, R; Manley, B. (2016) *Seismic response and engineering of cold-formed steel framed buildings*. Structures, Vol. 8, pp. 197-212). Elsevier.

[4] Papargyriou, I.; Mojtabaei, S.M.; Hajirasouliha, I.; Becque, J; Pilakoutas, K. (2022) *Cold-formed steel beam-to-column bolted connections for seismic*

applications. Thin-Walled Structures 172, 108876.

[5] Mojtabaei, S.M.; Becque, J; Hajirasouliha, I. (2021) *Behavior and Design of Cold-Formed Steel Bolted Connections Subjected to Combined Actions*. Journal of Structural Engineering, 147(4), p.04021013.

[6] Accorti, M.; Baldassino, N.; Zandonini, R.; Scavazza, F; Rogers, C.A. (2016) *Reprint of Response of CFS Sheathed Shear Walls*. Structures (Vol. 8, pp. 318-330). Elsevier.

[7] Eurocode, C.E.N. (2005) *3: design of steel structures, Part 1.3: General rules—supplementary rules for cold formed members and sheeting*. Brussels: European Committee for Standardization.

[8] Papargyriou, I.; Hajirasouliha, I.; Becque, J; Pilakoutas, K. (2021) *Performance-based assessment of CFS strap-braced stud walls under seismic loading*. Journal of Constructional Steel Research, 183, p.106731

[9] Badr, A.R.; Elanwar, H.H; Mourad, S.A. (2019) *Numerical and experimental investigation on cold-formed walls sheathed by fiber cement board*. Journal of Constructional Steel Research, 158, pp.366-380.

[10] Pan, C.L.; Shan, M.Y. (2011) *Monotonic shear tests of cold-formed steel wall frames with sheathing*. Thin-Walled Structures, 49(2), pp.363-370.

[11] Ye, J.; Wang, X.; Jia, H; Zhao, M. (2015) *Cyclic performance of cold-formed steel shear walls sheathed with double-layer wallboards on both sides*. Thin-Walled Structures, 92, pp.146-159.

[12] ABAQUS Inc.; Abaqus. (6.17) Computer-aided engineering, Finite Element Analysis Pawtucket, USA; 2017.

[13] Blais, C; Rogers, C.A. (2006) *Testing and design of light gauge steel frame 9mm OSB panel shear walls*. Eighteenth Int. Spec. Conf. Cold-Formed Steel Struct. Recent Res. Dev. Cold-Formed Steel Des. Constr., vol. 2006, pp. 637– 662, 2006.

[14] Kyvelou, P.; Gardner, L; Nethercot, D.A. (2017) *Testing and analysis of composite cold-formed steel and wood– based flooring systems*. Journal of Structural Engineering, 143(11), p.04017146.

[15] Kyprianou, C.; Kyvelou, P.; Gardner, L.; Nethercot, D.A. (2018) *Numerical study of sheathed cold-formed steel columns*. In 9th International Conference on Advances in Steel Structures (ICAAS'2018) (pp. 5-7).

[16] Peterman K.D.; Schafer B.W. *Hysteretic shear response of fasteners connecting sheathing to cold-formed steel studs*, CFS-NESS – RR04, 2013.

[17] Selvaraj, S.; Madhavan, M. (2020) *Structural behaviour and design of plywood sheathed cold-formed steel wall systems subjected to out of plane loading*. Journal of Constructional Steel Research, 166, p.105888.

[18] Hasanali, M.; Mojtabaei, S.M.; Clifton, G.C.; Hajirasouliha, I.; Torabian, S.; Lim, J.B.P. (2022) *Capacity and design of cold-formed steel warping-restrained beam-column elements*. Journal of Constructional Steel Research, 190, 107139.

[19] Schafer, B.W.; Li, Z; Moen, C.D. (2010) *Computational modeling of cold-formed steel*. Thin-walled structures, 48(10-11), pp.752-762.

[20] Schafer, B.W; Peköz, T. (1998) *Computational modeling of cold-formed steel: characterizing geometric imperfections and residual stresses*. Journal of constructional steel research, 47(3), pp.193-210.

[21] Hasanali, M.; Mojtabaei, S.M.; Hajirasouliha, I.; Clifton, G.C; Lim, J.B.P. (2023) *More accurate design equations for cold-formed steel members subjected to combined axial compressive load and bending*. Thin-Walled Structures 185, 110588.

[22] AISC, Seismic Provisions for Structural Steel Buildings, ANSI/AISC 341-16, 2016

[23] Gioncu, V. (2000) *Framed structures. Ductility and seismic response: General Report*. Journal of Constructional Steel Research, 55(1-3), pp.125-154.